Radiation of Mixed Layer Near-Inertial Oscillations into the Ocean Interior

J. MOEHLIS

Department of Physics, University of California, Berkeley, Berkeley, California

STEFAN G. LLEWELLYN SMITH

Department of Mechanical and Aerospace Engineering, University of California, San Diego, La Jolla, California

(Manuscript received 17 December 1999, in final form 28 August 2000)

ABSTRACT

The radiation from the mixed layer into the interior of the ocean of near-inertial oscillations in the presence of the beta effect is reconsidered as an initial-value problem. Making use of the fact that the mixed layer depth is much smaller than the total depth of the ocean, the solution is obtained in the limit of an ocean that is effectively infinitely deep. For a uniform initial condition, analytical results for the velocity, horizontal kinetic energy density, and fluxes are obtained.

This is the canonical solution for the radiation of near-inertial oscillations in the vertical, which captures the basic mechanisms due to the beta effect, and leads to the formation of small scales in the vertical. By superposing events, an average vertical wavenumber spectrum is constructed. The predicted decay of near-inertial mixed layer energy in the presence of the beta effect occurs on a timescale similar to that observed.

1. Introduction

There is much observational evidence, starting with Webster (1968) and Pollard and Millard (1970), that storms can excite near-inertial currents in the mixed layer of the ocean. This phenomenon is evident in observations from the Ocean Storms Experiment (D'Asaro et al. 1995; Levine and Zervakis 1995; Qi et al. 1995). Simple models that treat the mixed layer as a solid slab have been quite successful at explaining the process by which wind generates such currents [see, e.g., Pollard and Millard (1970); D'Asaro (1985)]. A weakness of the model of Pollard and Millard (1970) is that it explains the decay of these currents with an arbitrary decay constant. Much subsequent work has attempted to determine the detailed characteristics of this decay, with possible mechanisms including nonlinear interactions that transfer energy to other frequencies (Henyey et al. 1986), turbulent dissipation (Hebert and Moum 1994), and the radiation of downward propagating near-inertial oscillations (NIOs) excited by inertial pumping into the interior of the ocean (Gill 1984). NIOs are the portion of the oceanic internal wave field close to the Coriolis frequency and have been the subject of much interest recently (e.g., Garrett 2000). The downward radiation of NIOs will be the focus of this paper.

Corresponding author address: Dr. Jeff Moehlis, Program in Applied and Computational Mathematics, Princeton University, Fine Hall, Washington Rd., Princeton, NJ 08544-1000.
E-mail: jmoehlis@math.princeton.edu

Observations give a timescale on the order of 10–20 days for the decay of the energy deposited by the passing storm (D'Asaro et al. 1995; Levine and Zervakis 1995; Qi et al. 1995). This timescale stands in contrast with estimates, such as that by Gill (1984), that near-inertial currents decaying through the downward propagation of NIOs and with a horizontal length scale typical of the atmospheric forcing mechanism can remain in the mixed layer for longer than a year. To account for this difference, several mechanisms for the enhancement of vertical propagation of NIOs have been suggested. D'Asaro (1989) demonstrated that the β effect causes a reduction of horizontal scales because the meridional wavenumber evolves according to $l = l_0 - \beta t$, where l_0 is the initial wavenumber, and $l < 0$ corresponds to southward propagation. This accelerates the rate of inertial pumping of energy out of the mixed layer, thereby enhancing the decay of the NIOs. The decay is also enhanced through interaction with the background (quasi)geostrophic flow (e.g., Balmforth et al. 1998; van Meurs 1998; and Balmforth and Young 1999).

This paper reexamines the vertical propagation of near-inertial energy deposited into the mixed layer by a storm, in the presence of the β effect, using the formalism of Young and Ben Jelloul (1997) outlined in section 2. In section 3, a simplified model with three main assumptions is presented. First, there is no background flow. Second, the buoyancy frequency is taken to be constant and small in the mixed layer, and constant in the ocean interior beneath the mixed layer. Third, we

assume that the storm has moved rapidly across the ocean and has created a horizontally uniform near-inertial current to the east concentrated within the mixed layer; it is the subsequent evolution of this motion that is examined. Section 4 uses the fact that the depth of the ocean is very much larger than the mixed layer depth to formulate and solve the model for an ocean that is effectively infinitely deep. Section 5 constructs an average wavenumber spectrum due to the superposition of random events. Section 6 discusses the results and suggests directions for further investigation.

2. The NIO equation

We consider an ocean of infinite horizontal extent and depth D, with the mixed layer comprising the region $-H_{\text{mix}} < z < 0$, and the rest of the water column occupying $-D < z < -H_{\text{mix}}$. The x and y axes are taken to point to the east and north, respectively. The buoyancy frequency $N = N(z)$ is an arbitrary piecewise continuous function of depth z.

Young and Ben Jelloul (1997) derive an evolution equation for a complex field $A(x, y, z, t)$ that governs leading-order NIO motion in the absence of a background flow and in the presence of the β effect:

$$LA_t + \frac{i}{2} f_0 \nabla^2 A + i\beta y LA = 0, \tag{1}$$

where

$$LA = \frac{\partial}{\partial z}\left(\frac{f_0^2}{N^2}\frac{\partial A}{\partial z}\right), \tag{2}$$

and the Coriolis parameter is $f = f_0 + \beta y$. Here $\nabla^2 = \partial_x^2 + \partial_y^2$; subscripts denote partial differentiation. (See Young and Ben Jelloul (1997) and Balmforth et al. (1998) for the effect of a background flow.) The NIO velocity field (u, v, w), buoyancy b, and pressure p are given by

$$u + iv = e^{-if_0 t} LA, \tag{3}$$

$$w = -\frac{1}{2} f_0^2 N^{-2} (A_{xz} - iA_{yz}) e^{-if_0 t} + \text{c.c.}, \tag{4}$$

$$b = \frac{i}{2} f_0 (A_{xz} - iA_{yz}) e^{-if_0 t} + \text{c.c.}, \tag{5}$$

$$p = \frac{i}{2} (A_x - iA_y) e^{-if_0 t} + \text{c.c.} \tag{6}$$

The buoyancy b is related to the density ρ by

$$\rho = \rho_0 \left[1 - \frac{1}{g}\int_0^z N^2(z')\, dz' - \frac{b}{g}\right], \tag{7}$$

where ρ_0 is the reference density at the top of the ocean. The pressure p has been normalized by ρ_0.

The boundary conditions are that $A_z = 0$ at $z = 0$ and $z = -D$. This ensures that w vanishes at the top and bottom of the ocean. Using these boundary conditions,

$$\int_{-D}^{0} (u + iv) = 0. \tag{8}$$

Thus barotropic motion is not included in the analysis. However, Gill (1984) has shown that the barotropic response to a storm is instantaneous and the associated currents are weak.

3. A simplified model

Our analysis neglects the effect of the barotropic velocity and vorticity but crucially keeps the β effect. The initial NIO motion is taken to be uniform in x; hence A will remain independent of x. The buoyancy frequency profile is taken to be

$$N^2 = \begin{cases} \epsilon N_0^2 & \text{for } -H_{\text{mix}} < z < 0 \\ N_0^2 & \text{for } -D < z < -H_{\text{mix}}, \end{cases} \tag{9}$$

where $\epsilon \ll 1$. Finally, the storm is assumed to have produced an initial condition of a horizontally uniform near-inertial current to the east concentrated within the mixed layer. Instead of approaching this problem by use of an integral operator as in D'Asaro (1989) or by projecting onto normal modes (e.g., Gill 1984; Balmforth et al. 1998), the problem will be formulated as an initial value problem on a semi-infinite domain corresponding to an ocean that is effectively infinitely deep. In order to formulate the problem properly for this limit, this section considers an ocean of finite depth. In section 4 the solution in the limit in which the depth of the interior is much greater than the mixed layer depth will be found.

This formulation as a radiation problem that ignores the presence of the ocean bottom requires the projection of the initial condition to be spread across all the normal modes. This is certainly true for small mixed layer depths in the model of Gill (1984), as shown in Table 1 of that paper; see also Table 1 of Zervakis and Levine (1995). For deeper mixed layers, it is no longer true since half of the initial energy becomes concentrated in the first two or three modes. However, as pointed out in section 7 of Gill (1984), the depth of the ocean "influences the rate of loss of energy by imposing modulations on the rate, but the average rate of loss is not affected very much by depth changes." Hence the results presented here should be qualitatively relevant even when the continuum assumption is not valid.

a. Nondimensionalization

Quantities are nondimensionalized according to

$$\hat{y} = y/Y, \qquad \hat{z} = 1 + z/H_{\text{mix}}, \qquad \hat{t} = \Omega t,$$
$$\hat{N} = N/N_0, \tag{10}$$

where

$$Y \equiv \left(\frac{H_{\rm mix}^2 N_0^2}{\beta f_0}\right)^{1/3}, \qquad \Omega \equiv \left(\frac{\beta^2 H_{\rm mix}^2 N_0^2}{f_0}\right)^{1/3}. \quad (11)$$

This scaling corresponds to a balance of the tendency, dispersive, and beta terms so that all three enter the problem. Typical values $\beta = 10^{-11}$ m^{-1} s^{-1}, $H_{\rm mix} = 100$ m, $f_0 = 10^{-4}$ s^{-1}, $N_0 = 10^{-2}$ s^{-1} give $Y = 10^5$ m and $\Omega = 10^{-6}$ s^{-1}. The relevant timescale is thus $\Omega^{-1} =$ 11.5 days. The NIO velocity and field A are nondimensionalized by

$$(\hat{u}, \hat{v}) = \frac{(u, v)}{U}, \qquad \hat{A} = \frac{f_0^2}{UN_0^2H_{\rm mix}^2}A, \quad (12)$$

where U is a characteristic value of the initial NIO velocity.

The carets are now dropped for ease of notation. With this nondimensionalization, the buoyancy frequency profile is

$$N^2 = \begin{cases} \epsilon & \text{for } 0 < z < 1 \\ 1 & \text{for } -H \equiv 1 - D/H_{\rm mix} < z < 0, \end{cases} \quad (13)$$

and the NIO equation (1), the boundary conditions, and initial condition become

$$A_{zzt} + \frac{i}{2}N^2A_{yy} + iyA_{zz} = 0, \quad (14)$$

$$A_z = 0, \qquad z = -H, \quad z = 1, \quad (15)$$

$$A_{zz} = N^2(u + iv), \qquad t = 0. \quad (16)$$

The requirement that u and v remain finite implies the jump conditions

$$A_z|_{z=0^+} = \epsilon A_z|_{z=0^-}, \qquad A_{yy}|_{z=0^+} = A_{yy}|_{z=0^-}, \quad (17)$$

where $z = 0^+$ and $z = 0^-$ are the limits as $z \to 0$ from positive and negative values of z, respectively. The first condition comes from integrating (3) across the base of the mixed layer, while the second follows from this and (14).

This nondimensionalization allows some immediate conclusions to be drawn about the propagation of NIO energy downward. Most importantly, if $H_{\rm mix}$ increases, then the timescale Ω^{-1} decreases. Thus, assuming that the storm causes a uniform near-inertial current throughout the whole mixed layer, energy transfer will be faster for a deeper mixed layer. This confirms the results of Gill (1984), which associated the more efficient transfer with a larger projection of the initial velocity profile on the first vertical mode.

b. Boundary condition at the base of the mixed layer

Expanding $A(y, z, t) = A_0(y, z, t) + \epsilon A_1(y, z, t) + O(\epsilon^2)$ for $0 < z < 1$, (14) becomes, at $O(\epsilon^0)$,

$$A_{0zzt} + iyA_{0zz} = 0. \quad (18)$$

Integrating this subject to the boundary condition that A_z and A_{0z} vanish at $z = 1$ and using the property of the initial condition that $A = O(\epsilon)$ in the mixed layer, leads to the result that A_0 is independent of z. At $O(\epsilon)$,

$$A_{1zzt} + iyA_{1zz} + \frac{i}{2}A_{0yy} = 0, \quad (19)$$

which may be integrated subject to the boundary condition that A_{1z} vanishes at $z = 1$ to give

$$A_{1zt} + iyA_{1z} + \frac{i}{2}A_{0yy}(z - 1) = 0. \quad (20)$$

Evaluating at $z = 0^+$, and using $A_{yy} = A_{0yy} + O(\epsilon)$ and $A_z = \epsilon A_{1z} + O(\epsilon^2)$, gives

$$A_{zt} + iyA_z - \frac{i\epsilon}{2}A_{yy} = O(\epsilon^2), \qquad z = 0^+. \quad (21)$$

Finally, applying (17) gives the upper boundary condition for the NIO field in the ocean interior to leading order in ϵ:

$$A_{zt} + iyA_z - \frac{i}{2}A_{yy} = 0, \qquad z = 0^-. \quad (22)$$

Results obtained in the ocean interior using (22) are, in fact, leading-order solutions. We shall however use the notation A, even though it is really the leading-order term in the expansion.

c. Initial condition

The initial condition may be thought of as being generated by the rapid passage of a storm with a horizontal scale that is much larger than the scales under consideration. There is hence a uniform flow in the mixed layer, which we take to be to the east. For simplicity, the initial velocity is assumed to be piecewise constant with depth:

$$(u, v) = \begin{cases} (1, 0) & \text{for } 0 < z < 1 \\ (-H^{-1}, 0) & \text{for } -H < z < 0. \end{cases} \quad (23)$$

The weak flow in the ocean interior is necessary to ensure that the flow has no barotropic component. Integrating Eq. (16) with respect to z and using the boundary conditions (15) gives, at $t = 0$,

$$A_z = \begin{cases} \epsilon(z - 1) & \text{for } 0 < z < 1 \\ -(z + H)/H & \text{for } -H < z < 0. \end{cases} \quad (24)$$

4. Solution for an infinitely deep ocean

The total depth of the ocean is typically on the order of 100 times the depth of the mixed layer. Thus, the limit of infinite depth is considered. The initial condition is taken to be Eq. (24) with $H \to \infty$. The boundary condition for $z \to -\infty$ is taken to be $A_{zz} \to 0$, corresponding to the near-inertial velocities vanishing at infinite depth. Of course, this limit excludes the possibility

of reflections off the bottom of the ocean which may be important. Finally, the boundary condition for $z = 0^-$ given by Eq. (22) is used. Hence the problem to be solved for the semi-infinite domain $z < 0$ becomes

$$A_{zzt} + \frac{i}{2}A_{yy} + iyA_{zz} = 0, \qquad z < 0, \tag{25}$$

$$A_{zt} - \frac{i}{2}A_{yy} + iyA_z = 0, \qquad z = 0^-, \tag{26}$$

$$A_{zz} \to 0, \qquad z \to -\infty, \tag{27}$$

$$A_z = -1, \qquad t = 0. \tag{28}$$

a. NIO velocity field

The system (25)–(28) may be solved using transform techniques. Writing $A(y, z, t) = e^{-iyt}B(y, z, t)$, and Fourier transforming in y to give $\hat{B}(l, z, t)$, leads to the equations

$$\hat{B}_{zzt} - \frac{i}{2}(t - l)^2\hat{B} = 0, \qquad z < 0, \tag{29}$$

$$\hat{B}_{zt} + \frac{i}{2}(t - l)^2\hat{B} = 0, \qquad z = 0^-, \tag{30}$$

$$\hat{B}_{zz} \to 0, \qquad z \to -\infty, \tag{31}$$

$$\hat{B}_z = -\delta(l), \qquad t = 0. \tag{32}$$

Rewriting this system in terms of the new variable $T \equiv (t - l)^3/3$, which gives $\hat{B}_{zzt} = (t - l)^2\hat{B}_{zzT}$, leads to a set of equations where l only appears in the initial condition as the argument of a delta function. The solution will be proportional to this initial condition, and so the presence of the delta function in the inverse Fourier transform to recover B will lead to a solution $B(z, t)$ with no y dependence. We therefore take $A(y, z, t) = e^{-iyt}\tilde{B}(z, T)$ where $T = t^3/3$, and Eqs. (25)–(28) become

$$\tilde{B}_{zzT} - \frac{i}{2}\tilde{B} = 0, \qquad z < 0, \tag{33}$$

$$\tilde{B}_{zT} + \frac{i}{2}\tilde{B} = 0, \qquad z = 0^-, \tag{34}$$

$$\tilde{B}_{zz} \to 0, \qquad z \to -\infty, \tag{35}$$

$$\tilde{B}_z = -1, \qquad t = 0. \tag{36}$$

Defining the Laplace transform of $\tilde{B}(z, T)$ by

$$b(z, p) \equiv \mathcal{L}[\tilde{B}] \equiv \int_0^\infty \tilde{B}(z, T)e^{-pT}\,dT, \tag{37}$$

the governing equation (33) and the initial condition (36) become

$$pb_{zz} - \frac{i}{2}b = 0, \tag{38}$$

while the boundary conditions (34) and (35) become

$$pb_z + \frac{i}{2}b = -1, \qquad z = 0^-, \quad \text{and}$$

$$b_{zz} \to 0, \qquad z \to -\infty. \tag{39}$$

The solution to this system is

$$b(z, p) = -\frac{1}{\alpha}\frac{1}{\sqrt{p} + \alpha}\exp\left(\frac{\alpha z}{\sqrt{p}}\right). \tag{40}$$

where $\alpha \equiv (1 + i)/2$.

The Laplace transform (40) and its derivatives with respect to z must be inverted numerically for the ocean interior ($z < 0$). At the top of the ocean interior ($z = 0^-$) however, they may be obtained in closed form (using, e.g., Abramowitz and Stegun 1972). For example,

$$A_{zz}(y, 0^-, t) = e^{-iyt}\left[e^{it^3/6}\,\mathrm{erfc}\left(\frac{1 + i}{2\sqrt{3}}t^{3/2}\right) - 1\right]. \tag{41}$$

We now consider the back-rotated velocity $A_{zz} = e^{if_0t/\Omega}(u + iv)$, which filters out purely inertial motion at frequency f_0. Back-rotated velocities may be represented by hodographs that show the vector $(\mathrm{Re}(A_{zz}), \mathrm{Im}(A_{zz}))$ as curves parameterized by time. For $f_0 > 0$, if these curves are traced out in a clockwise (counterclockwise) fashion, the corresponding motion has frequency larger (smaller) than f_0. Figure 1 shows the back-rotated velocity at different locations. A common characteristic is that the magnitude of the back-rotated velocity starts at zero, reaches a peak value shortly after the storm, then decays away. The depth dependence of the back-rotated velocity is seen by comparing Figs. 1a and 1b, where both have $y = 0$ and thus the same value of the Coriolis parameter f. Qualitatively the results are the same, but closer to the mixed layer the direction change of the back-rotated velocity becomes slower, meaning that the frequency is closer to f_0. An idea of the latitudinal dependence is seen by comparing Figs. 1a, 1c, and 1d: at $y = 1$ the hodograph is traced out in a clockwise fashion as for $y = 0$, but at $y = -2$ it is traced out in a counterclockwise fashion.

b. Kinetic energy density and fluxes

The horizontal kinetic energy (HKE) per unit area contained within the mixed layer is, to leading order,

$$\int_0^1 dz\left|\frac{A_{zz}}{N^2}\right|^2 = \int_0^1 dz\left|\frac{A_{zz}}{\epsilon}\right|^2 = \int_0^1 dz|A_{1zz}|^2.$$

Expanding $\tilde{B}(z, T) = \tilde{B}_0(z, T) + \epsilon\tilde{B}_1(z, T) + O(\epsilon^2)$ in the mixed layer, (19) may be used to show that

$$pb_{1zz} - \tilde{B}_{1zz}(z, 0) - \frac{i}{2}b_0 = 0, \tag{42}$$

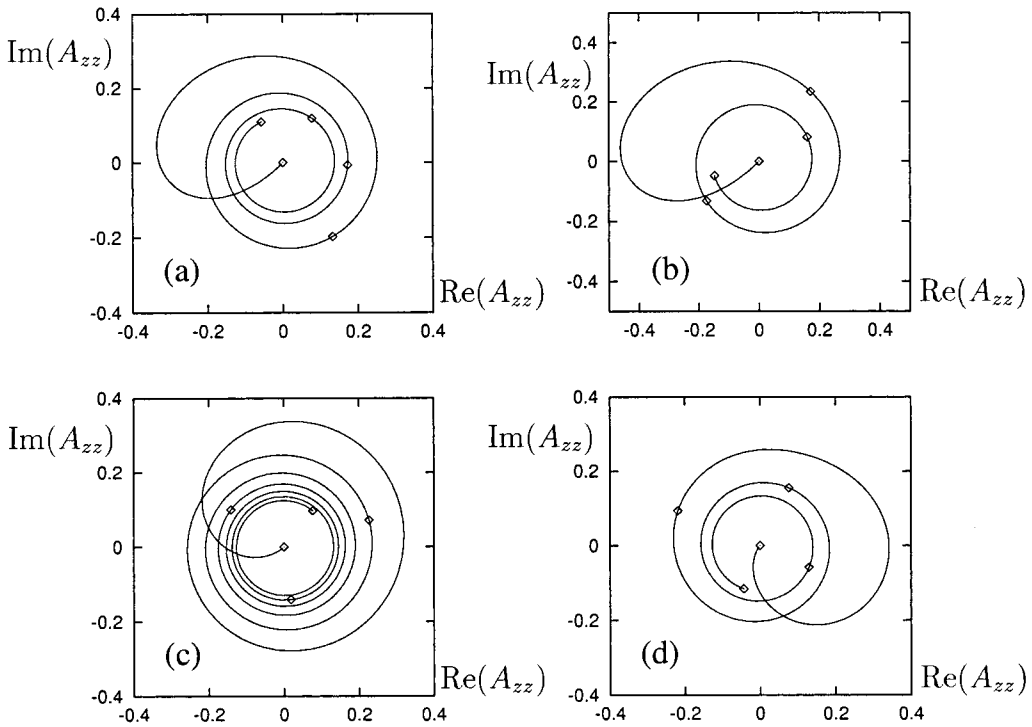

FIG. 1. Back-rotated velocity for (a) $z = -1$, $y = 0$; (b) $z = -0.5$, $y = 0$; (c) $z = -1$, $y = 1$; and (d) $z = -1$, $y = -2$. The diamonds are drawn at $t = 0, 5, 10, 15, 20$.

where $b_1 = \mathcal{L}[\tilde{B}_1]$ and $b_0 = \mathcal{L}[\tilde{B}_0]$. The initial condition within the mixed layer is $\tilde{B}_{1zz}(z, 0) = 1$ from (23). Now A is continuous across $z = 0$, and $\tilde{B}_0$ is independent of z in the mixed layer. Hence

$$b_{1zz} = \frac{1}{p} - \frac{i}{2\alpha p}\frac{1}{\sqrt{p} + \alpha}, \tag{43}$$

which may be inverted to give

$$A_{1zz}(y, t) = e^{-iyt}e^{it^{3/6}}\,\mathrm{erfc}\left(\frac{1 + i}{2\sqrt{3}}t^{3/2}\right). \tag{44}$$

Therefore the HKE within the mixed layer is

$$e_{\mathrm{ML}} \equiv \left|\mathrm{erfc}\left(\frac{1 + i}{2\sqrt{3}}t^{3/2}\right)\right|^2. \tag{45}$$

The time dependence of e_{ML} is shown in Fig. 2. Asymptotic results from Abramowitz and Stegun (1972) for the complementary error function imply that

$$e_{\mathrm{ML}} \sim 1 - \frac{2}{\sqrt{3\pi}}t^{3/2}, \qquad t \ll 1, \quad \text{and}$$

$$e_{\mathrm{ML}} \sim \frac{6}{\pi t^3}, \qquad t \to \infty. \tag{46}$$

Since the energy that leaves the mixed layer enters the interior of the ocean, this implies that for short times the energy in the interior increases like $t^{3/2}$. This does not contradict the result from D'Asaro (1989) that for short times the thermocline energy grows like t^6. That result assumes that the wind persists to generate a constant inertially oscillating velocity and that there is no propagating inertial motion. Here, the wind has an instantaneous effect, causing an initial horizontally uniform inertial current, and propagating inertial motion is included fully.

Another quantity of interest is the flux of HKE. Using (14) and its complex conjugate gives

$$\frac{\partial}{\partial t}\mathrm{HKE} = \frac{\partial}{\partial t}\left|\frac{A_{zz}}{N^2}\right|^2 = \frac{i}{2N^2}\frac{\partial}{\partial y}(A_{zz}A_y^* - A_{zz}^*A_y) + \frac{i}{2N^2}\frac{\partial}{\partial z}(A_{yz}^*A_y - A_{yz}A_y^*). \tag{47}$$

Assuming $A_{zz}A_y^* - A_{zz}^*A_y$ vanishes for $|y| \to \infty$ and using Eq. (15),

$$\frac{d}{dt}\int_{-H}^{-d} dz \int_{-\infty}^{\infty} dx \int_{-\infty}^{\infty} dy\, |A_{zz}|^2 = \int_{-\infty}^{\infty}\int_{-\infty}^{\infty} F_E(y, t; d)\, dx\, dy, \tag{48}$$

where

$$F_E(y, t; d) \equiv \frac{i}{2}(A_{yz}^*A_y - A_{yz}A_y^*)|_{z=-d} \tag{49}$$

gives the flux of HKE from the region $z > -d$ to the

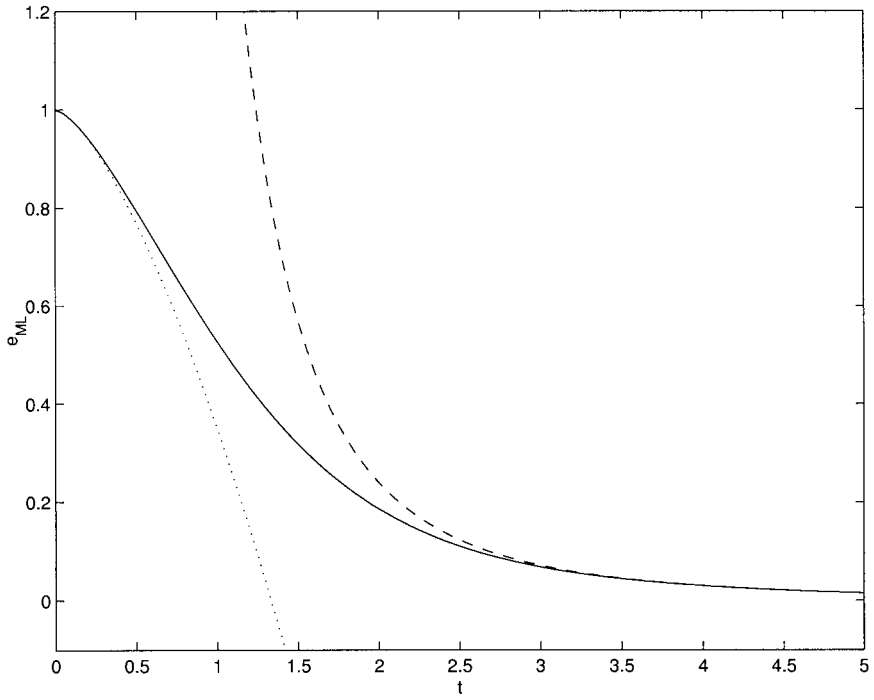

FIG. 2. HKE per unit volume in the mixed layer, e_{ML}. The solid curve shows the exact result and the dashed curves the asymptotic results for small and large times.

region $z < -d$. For this model, we consider the flux per unit area and hence discard the horizontal integrals. Integrating (48) with respect to time shows that the quantity

$$E(t; d) \equiv \int_0^t F_E \, dt \tag{50}$$

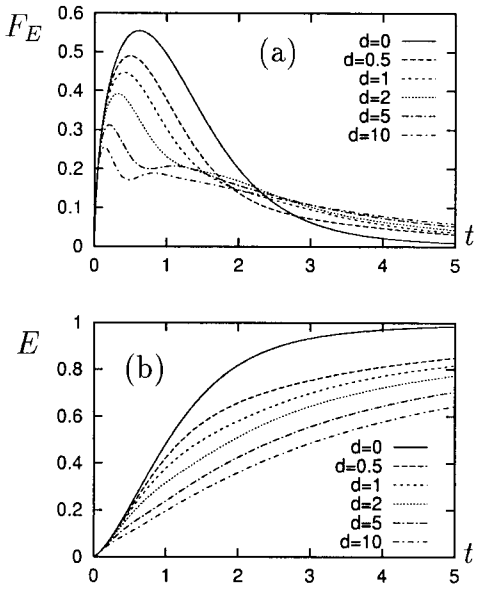

FIG. 3. (a) $F_E(t; d)$ and (b) $E(t; d)$ for different depths d below the base of the mixed layer. These show instantaneous and time-integrated fluxes of HKE.

gives the total amount of HKE (per unit area) that has penetrated into the region $z < -d$. Note that $E(t; d) \to 1$ corresponds to all the energy originally in the mixed layer having reached depths below $z = -d$. Results for $F_E(t; d)$ and $E(t; d)$ obtained by numerically inverting the appropriate Laplace transforms are shown in Fig. 3. The flux F_E peaks at the nondimensionalized time $t \approx 0.62$. For the typical values quoted in section 3a, this corresponds to a week after the storm. From Fig. 3b, and using the fact that whatever energy flows through $z = 0^-$ must have initially been in the mixed layer, we see that by $t = 1$ (about 11.5 days after the storm) nearly half of the energy associated with horizontal NIO currents caused by the storm has left the mixed layer; however, only about 38% of the total energy has penetrated below $z = -1$. By $t = 2$ (about 23 days after the storm), 82% of the total energy has left the mixed layer, but only 58% has penetrated below $z = -1$. Thus, at $t = 2$ nearly a quarter of the total energy is contained in the distance H_{mix} immediately beneath the mixed layer. This is reminiscent of the accumulation of NIO energy below the mixed layer seen in Balmforth et al. (1998). This model thus gives reasonable estimates for the timescale for which the decay of NIO energy occurs: for example, D'Asaro et al. (1995) found that the mixed layer inertial energy was reduced to background levels by 21 days after the storm.

Figure 4 shows the vertical dependence of the HKE and F_E at different times. As time increases the instantaneous distribution of HKE becomes more sharply peaked near the base of the mixed layer, but remains

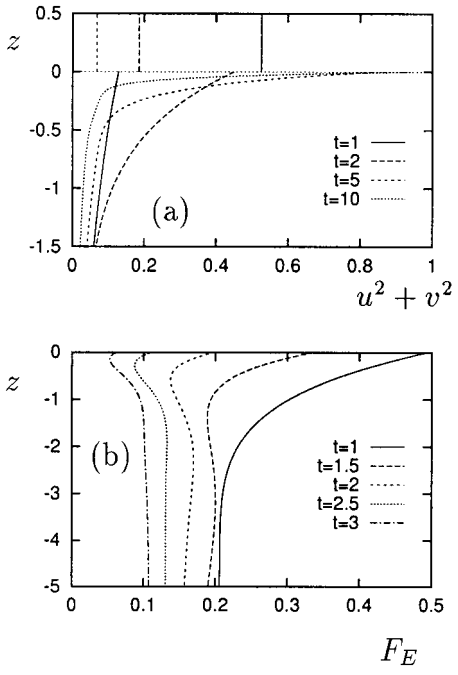

FIG. 4. Vertical profiles of (a) $u^2 + v^2$ and (b) $F_E(t, |z|)$ at $y = 0$ for different times showing the decay of energy from the mixed layer ($0 < z < 1$) and resultant behavior in the interior ($z < 0$). Note the different vertical scales.

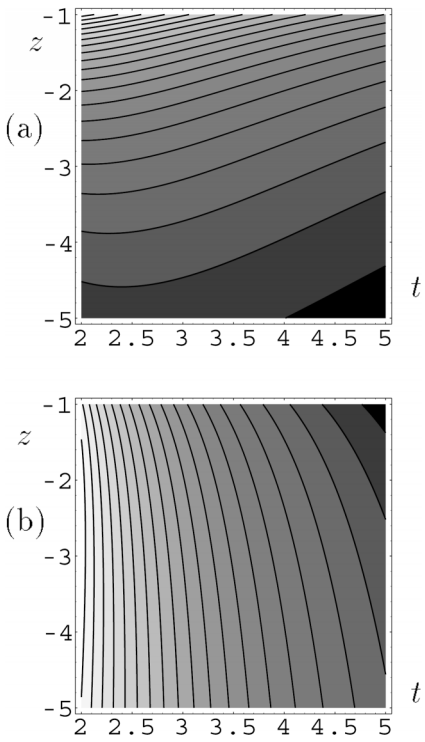

FIG. 5. Contour plots of the asymptotic results for (a) $u^2 + v^2$ and (b) F_E. Darker shading corresponds to smaller values.

bounded (asymptotically approaching unity) because of energy conservation. As in van Meurs (1998), the velocity step at the bottom of the mixed layer decreases at first; however, in our model this velocity step increases for larger times.

c. Large-time behavior

The asymptotic behavior of near-inertial properties may be derived using the method of steepest descents. The definitions

$$p \equiv (-z/T)^{2/3}w, \qquad \xi \equiv (z^2T)^{1/3},$$
$$\eta \equiv (-z/T)^{1/3} \tag{51}$$

take the inverse Laplace transform of b to the form

$$\tilde{B}(z, T) = -\frac{\eta^2}{2\pi\alpha i}\int_{\mathcal{B}} \frac{\exp[\xi(-\alpha/\sqrt{w} + w)]}{\eta\sqrt{w} + \alpha}\, dw, \tag{52}$$

where $\mathcal{B}$ is the Bromwich contour. The method of steepest descents can now be used to obtain the behavior of $\tilde{B}(z, T)$ and of its derivatives in the limit of large ξ (see appendix A). The result is that for large ξ, the back-rotated NIO velocity and the energy flux amplitude are given by

$$A_{zz} = e^{if_0t/\Omega}(u + iv)$$
$$\sim -\frac{1 + i\eta}{\pi(1 + \eta^2)}\sqrt{\frac{2\pi}{3}}\xi^{-1/2}e^{i(-3\xi/2+\pi/4)-iyt},$$
$$F_E \sim \frac{2\eta_0}{\pi(1 + \eta_0^2)t}, \tag{53}$$

respectively, where $\eta_0 = -(3z)^{1/3}/t$. A useful way to represent the asymptotic results is to draw contour plots of quantities of physical interest in the (z, t) plane; this is shown in Fig. 5. In the asymptotic limit for large ξ, with z constant, $u^2 + v^2$ and F_E decrease as time increases. Note that ξ is large for sufficiently large z and/or t, so good results can be obtained for large depths at quite small times.

d. Generation of small scales

The form of the asymptotic solution confirms what could have been predicted from the presence of the term $\tilde{B}_{zzT}$ in the governing equations, namely that for large times the vertical scale will decrease. Figure 6 shows the back-rotated NIO velocity components as a function of depth at $y = 0$ for two different times: $t = 1$ and $t = 8$. The formation of smaller vertical scales is very apparent.

The vertical shear in the interior can also be calculated using the steepest descents analysis, giving

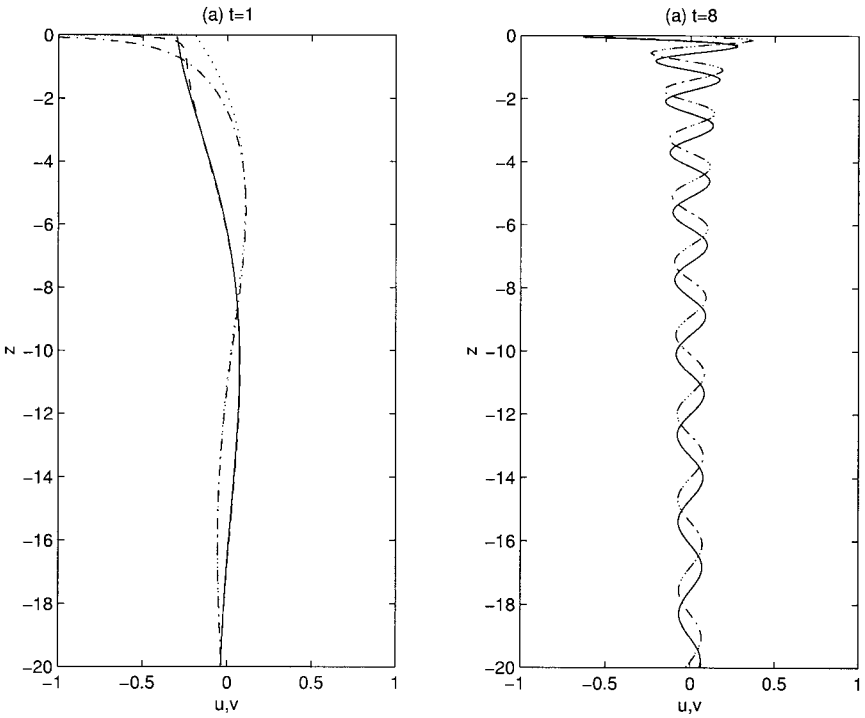

FIG. 6. Real and imaginary parts of the back-rotated NIO velocity $A_{zz} = e^{if_0 t/\Omega}(u + iv)$ (solid and dotted curves, respectively) and asymptotic approximations (dash and dash–dotted curves) for $y = 0$.

$$u_z^2 + v_z^2 = |A_{zzz}|^2 = |\tilde{B}_{zzz}|^2 \sim \frac{2}{\pi\eta_0^4(1 + \eta_0^2)t^3} \quad (54)$$

for large z^2t^3. At fixed depth $\eta_0 \sim 1/t$, so the Richardson number, $\mathrm{Ri} \equiv N^2/(u_z^2 + v_z^2)$, decreases with time, with $\mathrm{Ri} \sim 1/t$. Hence the static stability decreases, which could be important in the path to mixing: smaller vertical length scales could lead to overturning and localized mixing regions. The Richardson number is not necessarily a good indicator of static stability though since the flow has a vertical wavelike structure that is not captured by Ri.

The shear at the top of the ocean interior can be computed explicitly, however, since

$$b_{zzz}(0^-, p) = -\frac{\alpha^2}{p(p + \alpha\sqrt{p})}. \quad (55)$$

The inverse Laplace transform of this function may be calculated using results from Abramowitz and Stegun (1972), giving

$$A_{zzz}(y, 0^-, t) = e^{-iyt}\left[1 - e^{it^3/6}\,\mathrm{erfc}\left(\frac{1 + i}{2\sqrt{3}}t^{3/2}\right) - (1 + i)\sqrt{\frac{t^3}{3\pi}}\right]. \quad (56)$$

For large time, this leads to $u_z^2 + v_z^2 \sim t^3$ at the base of the mixed layer. Hence $\mathrm{Ri} \sim t^{-3}$ at the base of the mixed layer, and the flow becomes progressively less stable.

At $t = 0^+$, the shear is actually finite, even though the initial velocity was discontinuous. Thus, the unphysical nature of the initial condition is somewhat redeemed. The shear then grows in time, which suggests the possibility of mixing events being more and more likely to happen just below the mixed layer.

5. Vertical wavenumber spectrum

A natural quantity to compute using the above results is the vertical wavenumber spectrum. We consider the superposition of many wind events and compute the resulting average spectrum. The response calculated above, A, is causal and linear, so the result of superposing many such events will just be $\Sigma\, w_n A(t - t_n)$. Here t_n is the time at which an event occurs and the (complex) amplitude w_n gives the amplitude and direction of the initial wind input from the event.

To calculate an average spectrum, t_n was taken to come from a uniform distribution over a time interval $(0, T_m)$ with an average time between storms of τ. The total time interval T_m was taken to be 200 nondimensional time units, which is about 6 years, the average time between storms, τ, was taken to be 2 units or 23 days, and 100 realizations were carried out to obtain average values. The real and imaginary parts of the random amplitudes w_n were taken to be drawn from a

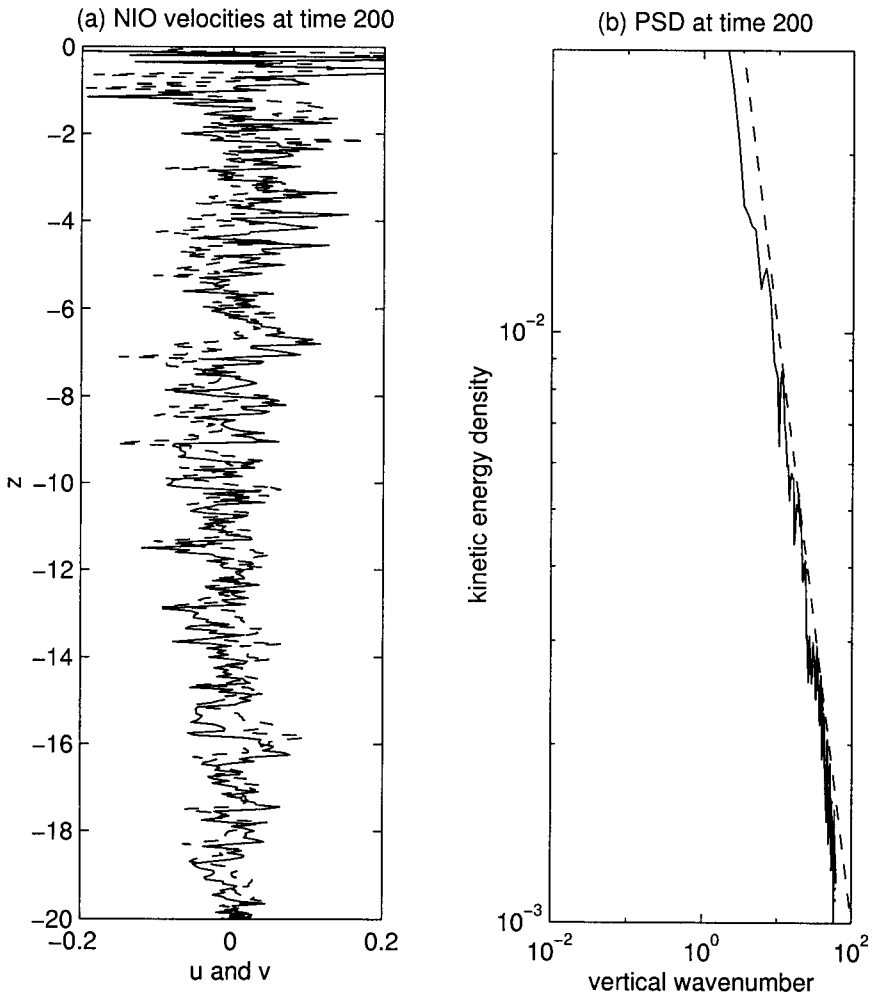

FIG. 7. (a) Average back-rotated NIO velocity $A_{zz} = e^{if_0t/\Omega}(u + iv)$ (real part solid, imaginary part dashed) after 200 time units averaged over 100 realizations. (b) Resulting power spectrum density calculated for downward-propagating waves using Welch's algorithm. The dots at the bottom show the largest upward propagating values and, hence, serve as an indicator for the numerical accuracy of the procedure. The dashed line has a slope of -1.

normal distribution with zero mean (the variance is irrelevant since the problem is linear).

Some way of taking into account dissipative processes such as the ones mentioned in the introduction is required: these processes contribute to a loss of NIO energy beyond that due to downward radiation, which is the only mechanism explicitly captured by the current model. Viscous processes would presumably lead to a scale-selective damping, while Newtonian damping would just lead to exponential decay. In the absence of any estimates for dissipation, damping was imposed by performing many realizations and then averaging. This is akin to calculating means over long times with the amplitude of each event decaying exponentially. The time interval T_m and number of realizations was found not to affect results significantly. Since one is interested in results over long times (in nondimensional units), the asymptotic form (53) can be used with very little loss in accuracy, especially since this approximation does well even for not so large times, provided z is not too small.

The power spectrum density of the resulting average NIO velocity field can then be calculated, as in D'Asaro and Perkins (1984). The N^2 stretching of the vertical coordinate is not required since N^2 is constant in the present model. The rotary decomposition of Leaman and Sanford (1975) was not carried out. Instead, the power spectrum density $|U_k|^2$ of $u + iv$ was calculated (at $y = 0$) from values of A between $z = -1.05$ and $z = -15$, that is, between 100 and 1500 m below the mixed layer, where observational data used to calculate spectra have been obtained. Welch's algorithm was used, as implemented by MATLAB'S PWELCH function, with eight overlapping data intervals and a Hamming filter. This gives the clockwise, downward propagating part of the spectrum separately from the counterclockwise,

upward propagating part of the spectrum; see Fig. 7. In this calculation, the latter component is essentially zero to within numerical accuracy.

The resulting spectral slope appears to be close to -1 rather than -3 as found in observations by Sanford (1991). The value of -1 is not an artifact of the technique in the sense that different values are obtained with synthetic data (i.e., other choices of A). This discrepancy might be resolved by taking into account other effects, such as the finite extent of storms, reflections from the ocean bottom, etc.

6. Conclusions

A simplified model has been developed to examine the decay due to the β effect of near-inertial currents excited in the mixed layer by a passing storm. This decay occurs due to the radiation of downward propagating NIOs into the interior of the ocean. The main assumptions of the model are that the background flow is zero, that the ocean has a simple (piecewise constant) buoyancy frequency profile, and that the storm has moved very quickly over the ocean causing a horizontally uniform near-inertial current concentrated in the mixed layer. The β effect is included in the analysis and is responsible for the radiation of NIOs. Because the depth of the mixed layer is much smaller than the total depth of the ocean, the problem is formulated in the limit of an effectively infinitely deep ocean. The resulting initial value problem can be solved by Laplace transforms. Analytical results are given for the horizontal kinetic energy density in the mixed layer, and results from the numerical inversion of the appropriate Laplace transforms are given for horizontal kinetic energy, energy flux, and back-rotated velocity. The asymptotic behavior is also investigated.

This is the canonical solution for the downward radiation of NIOs into the ocean interior and shows the formation of small-scale structures in the vertical. The magnitude of the shear increases in the ocean interior at constant depth. The shear at the base of the mixed layer is finite for $t > 0$ and also grows in time. Thus, one might expect overturning events to be triggered by the downward propagation of the NIOs.

The vertical wavenumber spectrum due to a superposition of random events can also be calculated. Energy clearly propagates downward, but the spectral slope of -1 does not correspond to observations. This suggests that some of the processes not considered in this approach are crucial for reproducing the observed behavior of the near-inertial portion of the oceanic internal wave spectrum.

Nevertheless, although this simplified model cannot be expected to capture the full complexity of the aftermath of a storm passing the ocean, it does capture much of the observed behavior. Most importantly, in the presence of the β effect the decay of near-inertial mixed layer energy is found to occur on the appropriate timescale (approximately 20 days), as in the analysis of D'Asaro (1989) and the observations by D'Asaro et al. (1995), Levine and Zervakis (1995), and Qi et al. (1995). The main advantage of the approach described in this paper is that many aspects of the decay in the mixed layer are analytically obtained for all times, unlike the approach of D'Asaro (1989) which predicts the timescale for the decay in a short time limit or estimates it in terms of the time it takes normal modes to become out of phase (cf. Gill 1984). Extensions to a more realistic ocean and storm would involve including a more realistic buoyancy frequency profile [e.g., the profile used by Gill (1984)], and considering the effect of different initial velocities (including both horizontal and vertical structure) and the effect of background flow. The study of all of these could use the same formalism of Young and Ben Jelloul (1997) and an approach similar to that presented here.

Acknowledgments. The majority of this work was carried out at the 1999 Geophysical Fluid Dynamics Summer School at the Woods Hole Oceanographic Institution. The authors would particularly like to thank W. R. Young for many useful discussions regarding this work. We acknowledge NSF Grant OCE-96-16017.

APPENDIX

Steepest-Descents Calculation

The argument of the exponential in (52) is the function $h(w) \equiv -\alpha/\sqrt{w} + w$. Using the principal branch of the square root, this function has saddle points at $w_1 = e^{-i\pi/2}/2$ and $w_2 = e^{5\pi i/6}/2$. The Bromwich contour can be deformed onto a contour of stationary phase that passes through both saddle points and the origin, avoiding the branch cut on the negative real axis. The asymptotic behavior for large ξ can now be computed.

The contribution from w_2 is exponentially small compared to that of w_1, so we may use the following formula for large $|\xi|$:

$$I(\xi) \equiv \int_{\mathcal{B}} f(w)e^{\xi h(w)}\,dw \sim \left(\frac{2\pi}{|\xi h''(w_1)|}\right)^{1/2} f(w_1)e^{\xi h(w_1)}e^{i\gamma}, \qquad \text{(A1)}$$

where γ is the angle at which the path passes through the saddle. Here $\gamma = \pi/4$, so for large $|\xi|$, we have

$$\tilde{B} \sim \frac{\eta^2(1 + i\eta)}{\pi(1 + \eta^2)}\sqrt{\frac{2\pi}{3}}\xi^{-1/2}e^{i(-3\xi/2+\pi/4)}. \qquad \text{(A2)}$$

An almost identical calculation leads to asymptotic behaviors for $\tilde{B}_z$ and $\tilde{B}_{zz}$, which take the form

$$\frac{\eta(i - \eta)}{\pi(1 + \eta^2)}\sqrt{\frac{2\pi}{3}}\xi^{-1/2}e^{i(-3\xi/2+\pi/4)} \quad \text{and}$$

$$-\frac{1 + i\eta}{\pi(1 + \eta^2)}\sqrt{\frac{2\pi}{3}}\xi^{-1/2}e^{i(-3\xi/2+\pi/4)}, \qquad \text{(A3)}$$

respectively.

REFERENCES

Abramowitz, M., and I. A. Stegun, 1972: *Handbook of Mathematical Functions*. Dover Press, 1046 pp.

Balmforth, N. J., and W. R. Young, 1999: Radiative damping of near-inertial oscillations in the mixed layer. *J. Mar. Res.*, **57,** 561–584.

——, S. G. Llewellyn Smith, and W. R. Young, 1998: Enhanced dispersion of near-inertial waves in an idealized geostrophic flow. *J. Mar. Res.*, **56,** 1–40.

D'Asaro, E. A., 1985: The energy flux from the wind to near-inertial motions in the surface mixed layer. *J. Phys. Oceanogr.,* **15,** 1043–1059.

——, 1989: The decay of wind-forced mixed layer inertial oscillations due to the β effect. *J. Geophys. Res.,* **94,** 2045–2056.

—— and H. Perkins, 1984: A near-inertial internal wave spectrum for the Sargasso Sea in late summer. *J. Phys. Oceanogr.,* **14,** 489–505.

——, C. C. Eriksen, M. D. Levine, P. Niiler, C. A. Paulson, and P. van Meurs, 1995: Upper-ocean inertial currents forced by a strong storm. Part I: Data and comparisons with linear theory. *J. Phys. Oceanogr.,* **25,** 2909–2936.

Garrett, C., 2000: What is the ''near-inertial'' band and why is it different? *Dynamics of Oceanic Internal Gravity Waves, II, Proc. 'Aha Huliko'a Hawaiian Winter Workshop,* P. Müller and D. Henderson, Eds., SOEST, 215–221.

Gill, A. E., 1984: On the behavior of internal waves in the wakes of storms. *J. Phys. Oceanogr.,* **14,** 1129–1151.

Hebert, D., and J. N. Moum, 1994: Decay of a near-inertial wave. *J. Phys. Oceanogr.,* **24,** 2334–2351.

Henyey, F. S., J. A. Wright, and S. M. Flatté, 1986: Energy and action flow through the internal wave field: An eikonal approach. *J. Geophys. Res.,* **91,** 8487–8495.

Leaman, K. D., and T. B. Sanford, 1975: Vertical energy propagation of inertial waves: A vector analysis of velocity profiles. *J. Geophys. Res.,* **80,** 1975–1978.

Levine, M. D., and V. Zervakis, 1995: Near-inertial wave propagation into the pycnocline during ocean storms: Observations and model comparison. *J. Phys. Oceanogr.,* **25,** 2890–2908.

Pollard, R. T., and R. C. Millard Jr., 1970: Comparison between observed and simulated wind-generated inertial oscillations. *Deep-Sea Res.,* **17,** 813–821.

Qi, H., R. A. De Szoeke, C. A. Paulson, and C. C. Eriksen, 1995: The structure of near-inertial waves during ocean storms. *J. Phys. Oceanogr.,* **25,** 2853–2871.

Sanford, T. B., 1991: Spatial structure of thermocline and abyssal internal waves. *Dynamics of Oceanic Internal Gravity Waves, Proc. 'Aha Huliko'a Hawaiian Winter Workshop,* P. Müller and D. Henderson, Eds., SOEST, 109–141.

van Meurs, P., 1998: Interactions between near-inertial mixed layer currents and the mesoscale: The importance of spatial variabilities in the vorticity field. *J. Phys. Oceanogr.,* **28,** 1363–1388.

Webster, F., 1968: Observation of inertial-period motions in the deep sea. *Rev. Geophys.,* **6,** 473–490.

Young, W. R., and M. Ben Jelloul, 1997: Propagation of near-inertial oscillations through a geostrophic flow. *J. Mar. Res.,* **55,** 735–766.

Zervakis, V., and M. D. Levine, 1995: Near-inertial energy propagation from the mixed layer: Theoretical consideration. *J. Phys. Oceanogr.,* **25,** 2872–2889.